

ALMA Host galaxy observation of the off-axis Gamma-Ray Burst XRF 020903

JHENG-CYUN CHEN,¹ YUJI URATA,¹ AND KUIYUN HUANG²

¹*Institute of Astronomy, National Central University, Chung-Li 32054, Taiwan*

²*Center for General Education, Chung Yuan Christian University, Taoyuan 32023, Taiwan*

(Received January 28, 2021; Revised April 28, 2021; Accepted May 11, 2021)

ABSTRACT

We investigated the radio properties of the host galaxy of X-ray flash, XRF 020903, which is the best example for investigating of the off-axis origin of gamma-ray bursts (GRBs). Dust continuum at 233 GHz and CO are observed using the Atacama Large millimeter/submillimeter array. The molecular gas mass derived by applying the metallicity-dependent CO-to-H₂ conversion factor matches the global trend along the redshift and stellar mass of the GRB host galaxies. The estimated gas depletion timescale (pertaining to the potential critical characteristics of GRB host galaxies) is equivalent to those of GRBs and super-luminous supernova hosts in the same redshift range. These properties of the XRF 020903 host galaxy observed in radio resemble those of GRB host galaxies, thereby supporting the identical origin of XRF 020903 and GRBs.

Keywords: gamma rays: bursts — gammarays: observation

1. INTRODUCTION

X-ray flashes (XRFs) were discovered by the BeppoSAX satellite during the dawn of the gamma-ray bursts (GRBs; Heise et al. 2001; Kippen et al. 2002). The observed X-ray properties in the prompt phase were identical to those of GRBs, except for the considerably lower energy values of the spectral peak energy, E_{peak} in the νF_{ν} spectrum. Systematic prompt phase observations made by HETE-2 indicated that the XRFs are associated with the same phenomenon as classical hard GRBs and are representative of the extension of the GRB population to low-peak-energy events (Sakamoto et al. 2005). Three models have been proposed to explain the observed prompt properties: high-redshift origin (Heise 2003), intrinsic property (e.g., a subenergetic or inefficient fireball; Huang et al. 2002), and off-axis jet models (Yamazaki et al. 2002; Zhang et al. 2004; Lamb et al. 2005). For the latter two models, on-axis and off-axis orphan GRB afterglows can appear because of their lower Lorentz factor caused by inefficient fireball and off-axis viewing, respectively. Urata et al. (2015) confirmed the off-axis origin of the XRF 020903 case by identifying achromatic rebrightening in the afterglow. Additionally, XRF 020903 was characterized well through observations, e.g., redshift measurement (Soderberg et al. 2004), a lower intrinsic $E_{\text{peak}}^{\text{src}}$ (Sakamoto et al. 2004), and supernova association (Soderberg et al. 2005). Among all

the XRF samples, XRF 020903 was the only sample suitable for investigating its origin. Although the XRF observations have been terminated owing to the lack of wide-field soft-X-ray monitoring instruments such as WXM on board HETE-2 (Shirasaki et al. 2003), planned GRB missions, i.e., SVOM (Godet et al. 2012), HiZ-GUNDAM (Yonetoku et al. 2020), and THESEUS (Amati et al. 2018) would provide large samples.

The off-axis viewing of GRB jets for both long and short GRBs is essential for understanding the unification of GRBs, including related energetic stellar explosions, as well as to perform multimessenger astronomy. In particular, short GRBs and the jet viewing angle are essential for understanding the characteristics of short GRBs associated with the gravitational wave transients caused by neutron star mergers (e.g., Alexander et al. 2017; Haggard et al. 2017; Lazzati et al. 2017; Murguia-Berthier et al. 2017; Ioka, & Nakamura 2018; Jin et al. 2018; Kathirgamaraju et al. 2018; Troja et al. 2018, 2019; Lamb & Kobayashi 2018; Lyman et al. 2018; Lamb et al. 2019). Long GRBs are believed to occur when a very massive star dies in a highly energetic supernova (SNe), forming a black hole and producing a relativistic jet. The averaged jet opening angles were measured to be $\sim 3^{\circ}.5$, i.e., of the same order as that of AGNs, based on achromatic temporal breaks in afterglow light curves (e.g., Racusin et al. 2009). Cocoon

structures surrounding the GRB jets were identified to be similar to those of AGNs (Izzo et al. 2019; Chen et al. 2020). Similar to the unification model of AGNs, observing GRB jets at the various viewing angles can provide GRBs, XRFs, off-axis orphan GRB afterglows, and energetic stellar explosions (e.g., Pastorello et al. 2010; Huang et al. 2019; Izzo et al. 2020). In this regard, all of these phenomena share the same environment (i.e., common host galaxy properties).

Off-axis orphan GRB afterglow searches were performed at various wavelengths (Grindlay 1999; Greiner et al. 2000; Rau et al. 2006; Levinson et al. 2002; Gal-Yam et al. 2006; Huang et al. 2020). Although these numerous surveys do not involve the detection of off-axis orphan GRB afterglows, the detection rate implies that the consideration of jet structures is essential for future orphan GRB afterglow surveys (e.g., Huang et al. 2020). The VLA Sky Survey (VLASS) identified a luminous radio transient and reported it as a candidate for off-axis orphan GRB afterglows (Law et al. 2018; Marcote et al. 2019). Although the possibility of the nebula of a newly born magnetar is not precluded, the similar star formation property of the host galaxy to that of long GRB hosts supports the off-axis orphan GRB afterglow phenomenon.

Millimeter and submillimeter observations for both GRBs and their host galaxies using the Atacama Large Millimeter/submillimeter Array (ALMA) have provided new insights. The first measurement of the radio linear polarization suggested depolarization caused by nonenergetic electrons, which afforded acceleration efficiency at the shock (Urata et al. 2019). Meanwhile, carbon monoxide (CO) lines (Hatsukade et al. 2014; Arabsalmani et al. 2020) were identified from spatially resolved imaging observation. Hatsukade et al. (2014) indicated that the bursts occurred in regions rich in dust, but not particularly rich in molecular gas. Arabsalmani et al. (2020) revealed that the presence of starburst modes of star formation on local scales in the galaxy, even though the galaxy as a whole cannot be categorized as a starburst based on its global properties. By expanding the previous studies using nearby GRB samples ($z < 0.12$; Michałowski et al. 2018), statistical studies regarding CO observations indicated possible common properties of GRB host galaxies in terms of their molecular gas mass fraction and gas depletion timescale, particularly at $z < 1$ (Michałowski et al. 2018; Hatsukade et al. 2020a). Additionally, the detection of [C II] also provided a new physical property for the characterization of GRB host galaxies at $z \sim 1 - 2$ (Hashimoto et al. 2019).

Herein, we present the results of ALMA continuum and CO line observations on the host galaxy of an off-axis GRB event (i.e., XRF 020903). The remainder of this paper proceeds as follows. In Section 2, we summarize the previous XRF 020903 observations. In Section 3, we describe the ALMA observations for XRF 020903 host galaxies and other GRB samples. In Sections 4 and 5, we present the results of the continuum and CO line observations and discuss their properties, respectively, based on using the following cosmological parameters: $H_0 = 70 \text{ km s}^{-1}$, $\Omega_0 = 0.3$, and $\Omega_\lambda = 0.7$.

2. OFF-AXIS GRB, X-RAY FLASH 020903

XRF 020903 is the most favorable sample for the unification of GRBs, whereas the jet viewing angle is the most favorable parameter. The event was characterized by (a) measurements of lower spectral peak energy of the prompt emission, (b) redshift measurements ($z = 0.251$), (c) evidence of the off-axis viewing of the GRB jet, (d) association of a supernova component in the optical afterglow, and (e) a low-metallicity environment via an optical identification of the host galaxy. Based on observation by the HETE-2 satellite, the lowest intrinsic spectral peak energy $E_{\text{peak}}^{\text{src}}$ of $3.3_{-1.0}^{+1.8} \text{ keV}$ was identified among all the XRF samples (Sakamoto et al. 2004). The redshift of $z = 0.251$ (Soderberg et al. 2004) was measured via optical spectroscopic observation observations. Achromatic rebrightening caused by the off-axis viewing of classical GRB jets (Urata et al. 2015) were detected via early multicolor optical observations. SN1998bw-like supernova association was confirmed via optical spectroscopy at ~ 25 day after the burst (Soderberg et al. 2005).

The high-resolution host galaxy image obtained by the Hubble Space Telescope (HST; Soderberg et al. 2004) shows the existence of at least four components as shown in Figure 1. The optical spectroscopy for the burst site measured the metallicities as $\log(\text{O}/\text{H}) + 12 \sim 8.0$. Combined with GRB host galaxy measurements, the observed metallicities indicated the lowest values (Levesque et al. 2010). Meanwhile, burst site studies involving optical spectra also indicated features of a significant Wolf-Rayet star population (Hammer et al. 2006; Han et al. 2010). The spatially resolved optical spectroscopic observations indicated that the burst site is likely the most recent and active site of star formation in the XRF 020903 host galaxy, which is consistent with other spatially resolved GRB host galaxy studies (Thorp & Levesque 2018). Using line diagnostics (Thorp & Levesque 2018), the low metallicities for all of four regions were measured to be 8.1 ± 0.1 for the burst site and ~ 8.2 for the remaining regions.

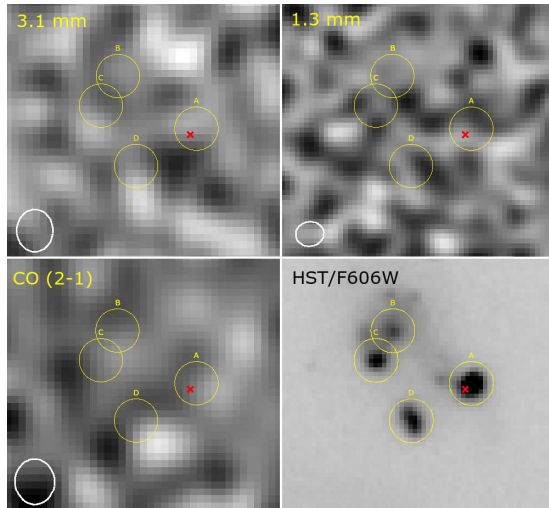


Figure 1. Continuum maps at 3.1 mm (top left) and 1.3 mm (top right), CO velocity-integrated maps (bottom left), and optical image (bottom right). The yellow circles with $0''.2$ radius indicate the positions of optical components. Afterglow position is marked by the red cross. Synthesized beam size is shown in the lower left corners.

3. OBSERVATIONS AND DATA

3.1. XRF 020903

The location of the XRF 020903 field at Band 3 and Band 6, for the Cycle 3 program (Project code: 2015.1.01254.S) was observed using ALMA. The observations in Band 3 were executed on 2016 September 19 and 21. The total on-source time was 4318 s. A correlator was used in the frequency domain mode with a bandwidth of 1875 MHz ($488.28 \text{ kHz} \times 3840 \text{ channels}$). Four basebands were used, resulting in a total bandwidth of 7.5GHz. The main aspect of the observation was the search for the CO ($J = 1 - 0$) line associated with the XRF 020903 host galaxy. The bandpass and flux were calibrated using observations from J2258-2758 and J0006-0623, and those from J2236-1433 were used for the phase calibration. The photometric observation in Band 6 with the total on-source time of 962 s was performed on 2016 July 28. The bandpass and flux were calibrated using observations from J2258-2758 and Pallas, whereas observations from J2303-1841 were used for phase calibration.

The data were reduced using the Common Astronomy Software Applications package (McMullin et al. 2007) in a standard manner. Data calibration was performed using the ALMA Science Pipeline Software of CASA version 4.7.0-1. Maps were processed using the TCLEAN algorithm with the Briggs weighting (with a robust parameter of 0.5). Furthermore, a CO ($J = 1 - 0$) velocity-integrated map with a velocity width of 180 km s^{-1} was

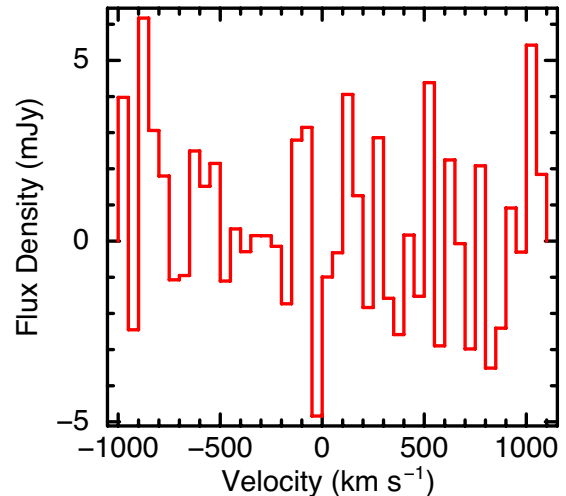


Figure 2. CO spectra with the velocity resolution of 47.7 km s^{-1} for the burst site of the XRF 020903.

created using the TCLEAN algorithm. The final synthesized beam size (FWHM) was $0''.38 \times 0''.33$ for Band 3, $0''.27 \times 0''.23$ for Band 6, and $0''.42 \times 0''.36$ for the velocity-integrated maps. These maps, with their optical images obtained using the HST, are shown in Figure 1. By resolving the four optical host galaxy components, the 3σ upper limits of 0.032 mJy at 113 GHz and 0.061 mJy at 224 GHz were estimated. The 3σ limit of the CO velocity-integrated map with 180 km/s was 0.57 mJy. The spectra around the CO($J = 1 - 0$) line for the host region was centered at R.A. = $22^h 48^m 42^s.37$, decl. = $-20^\circ 46' 08''.72$ with a radius of $0''.8$ (i.e., including all four optical components) indicates a null detection (Figure 2).

3.2. GRB Host Galaxy Samples

Table 1 summarizes the properties of 36 GRBs and two super-luminous supernova (SLSN) host galaxies observed using the ALMA in comparison with the XRF 020903 measurements. These samples included various GRBs, including one short GRB (GRB 050709; Hjorth et al. 2005; Villaseñor et al. 2005; Fox et al. 2005) and one ultra-long GRB (GRB 130925A; Bellm et al. 2014; Piro et al. 2014; Evans et al. 2014). GRB 050709 is a classical short/hard GRB, but the optical properties of its host galaxy indicate star formation activity (Covino et al. 2006). GRB 130925A is also classified as an optically dark GRB because of its high visual extinction (Greiner et al. 2014). The revised redshift (Perley et al. 2017) is used for one of the optically dark GRBs, GRB 020819B for evaluating the observation targeted on the CO line. Two samples (GRB 090423 and GRB 130606A) may have occurred at the reionization epoch (e.g., Tanvir et al. 2009; Totani et al.

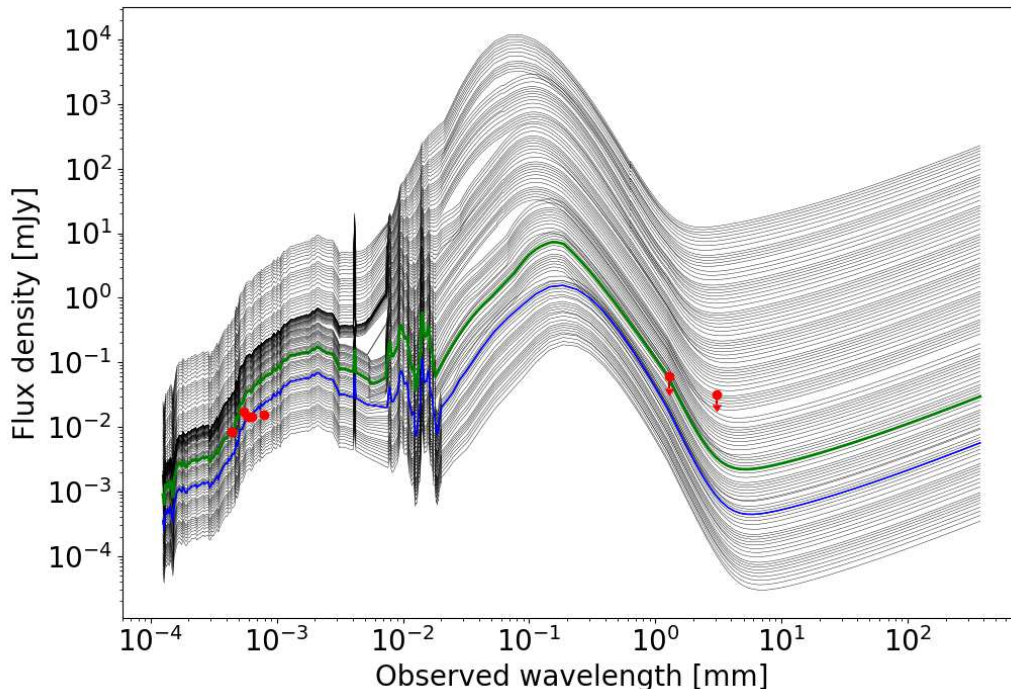


Figure 3. SED of the XRF 020903 host galaxy. The ALMA observation constrains the IR SEDs using template scaling. Templates lower than the green solid line satisfy the ALMA 3σ upper limit for the XRF 020903 host galaxy. The solid blue line is the closest to the optical measurement based on the high-resolution image captured using HST.

2014, 2016). The neutral fraction of the IGM measured using GRB 130606A implied the incompleteness of reionization at $z \sim 6$ (Totani et al. 2014, 2016). This higher redshift event also obeys the energy correlations established using low-redshift GRBs (Yasuda et al. 2017). Furthermore, we added two SLSNs (i.e., SN2017egm and PTF10tpz), as potential samples of identical stellar explosions by observing the GRB jet at an off-axis viewing angle (e.g., Nicholl et al. 2017; Wheeler et al. 2017; Coppejans et al. 2018).

These physical properties of the reference samples were obtained by reducing the ALMA archive data and from the literature. We used the products obtained from the ALMA archive for continuum observations, except for GRB 050709. These archive data were calibrated and imaged by the ALMA Regional Centers using standard procedures. Two execution blocks for GRB 050709 observations (Project code: 2016.1.01333.S) at the identical band (Band 6) were reduced separately. We reproduced the calibrated data, merged them, and then imaged them using TCLEAN. The total flux measurements and the RMS noise estimations for the nondetection cases were performed using function "imfit" and "imstat", respectively. We confirmed that our continuum measurements

were consistent with previous results (Wang et al. 2012; Huang et al. 2017; Berger et al. 2014; Hatsukade et al. 2020a). For Table 1, we referred to the detailed measurements made by Endo et al. (2007), Hatsukade et al. (2011), Wang et al. (2012), Berger et al. (2014), Hatsukade et al. (2014), Stanway et al. (2015), Huang et al. (2017), Michałowski et al. (2018), Arabsalmani et al. (2019), Hashimoto et al. (2019), Hatsukade et al. (2019), de Ugarte Postigo et al. (2020), Hatsukade et al. (2020a), and Hatsukade et al. (2020b).

4. IR LUMINOSITY AND STAR FORMATION RATE (SFR) WITH GRB HOST GALAXIES

The ALMA continuum observations provided unique upper limits for estimating the rest-frame IR luminosity and SFR of GRB and XRF host galaxies. Based on Wang et al. (2012), a redshift to a template IR SED was applied to these results. We referred to the SED library provided by Chary & Elbaz (2001), which is luminosity-dependent (2×10^8 to $4 \times 10^{13} L_{\odot}$) based on a locally calibrated luminosity-dust temperature relation and does not enable SED scaling. As shown in Figure 3, we constrained the 3σ upper limits of IR luminosity for the XRF 020903 host galaxy with the Band 6 obser-

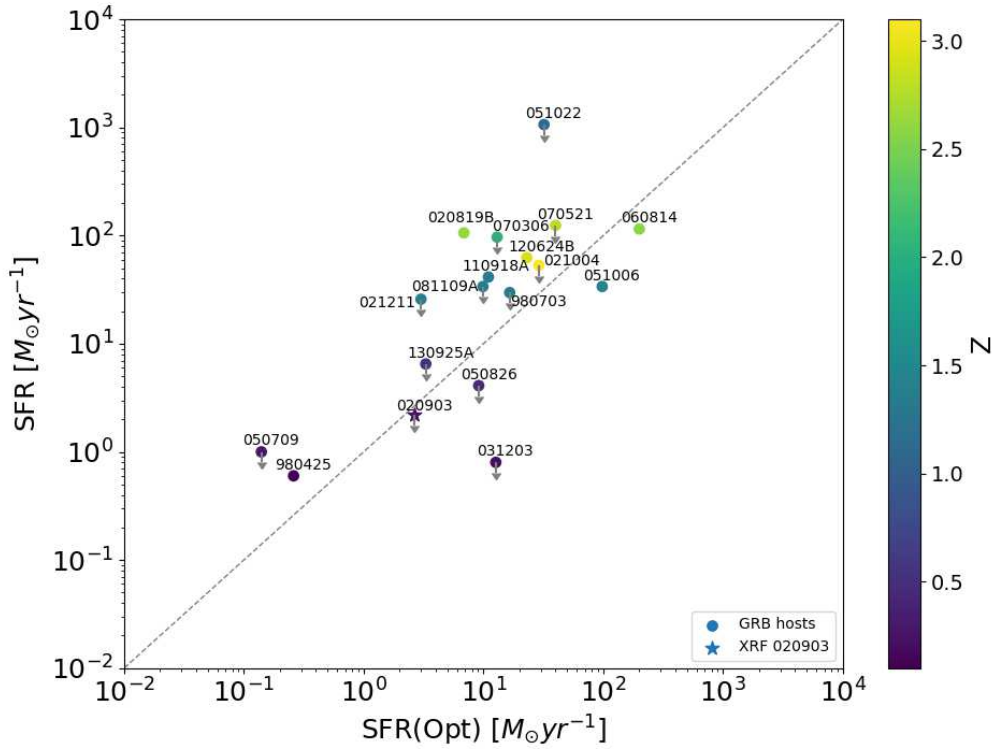


Figure 4. The SFRs obtained using the SED template scaling method compared with the measurements obtained using the optical method (i.e., emission lines or UV luminosity; Savaglio et al. 2009).

variation as $L_{\text{IR}} < 1.3 \times 10^{10} L_{\odot}$. Moreover, the templates with $L_{\text{IR}} < 1.3 \times 10^{10} L_{\odot}$ are also consistent with optical flux measurements (the blue line in the Figure 3). In terms of the SED for describing optical measurements, we primarily used the HST measurement (Soderberg et al. 2004), because the ground-based multicolor measurements were affected by the nearby galaxies, as reported by Bersier et al. (2006). Using the SFR conversion of star-forming galaxies, $\text{SFR}(M_{\odot} \text{ yr}^{-1}) = 1.7 \times 10^{-10} L_{\text{IR}}/L_{\odot}$ (Kennicutt 1998), we obtained the 3σ upper limit of the SFR as $< 2.2 (M_{\odot} \text{ yr}^{-1})$. This estimation is consistent with the measurement ($2.65 M_{\odot} \text{ yr}^{-1}$) using H_{α} or rather small (Savaglio et al. 2009).

Similarly, we derived the L_{IR} and SFR for reference GRB samples (Table 1). Figure 4 shows a comparison between the estimated SFRs and those measured based on H_{α} , $[\text{OII}]$ or UV fluxes (Savaglio et al. 2009). The SFR estimation for the XRF 020903 host obtained using the L_{IR} method was one of the notable events that exhibited smaller values than the optical measurements, similar to GRB 031203 ($z = 0.105$), GRB 050826 ($z = 0.296$), GRB 051006 ($z = 1.059$), and GRB 060814 ($z = 1.923$). This result indicates that the low dust content of the GRB host galaxies. Because the lower opti-

cal depth of the dust tends to increase the SFR conversion coefficient (e.g., Buat & Xu 1996; Kennicutt 1998), an empirical calibration of SFR/L_{IR} is required based on other physical parameters, such as stellar mass and metallicity.

5. LIMIT OF LUMINOSITY OF CO AND MOLECULAR GAS

5.1. Molecular Gas Mass

The luminosity of CO was estimated based on the equation ($L'_{\text{CO}} = 3.25 \times 10^7 S_{\text{CO}} \Delta \nu \nu_{\text{obs}}^{-2} D_L^2 (1+z)^{-3}$) described by Solomon and Vanden Bout (2005), where L'_{CO} is in $\text{K km s}^{-1} \text{ pc}^2$, $S_{\text{CO}} \Delta \nu$ is the velocity-integrated intensity in Jy km s^{-1} , ν_{obs} is the observed line frequency in GHz , and D_L is the luminosity distance in Mpc . Because the CO(1-0) line was not detected from the ALMA observation of the XRF 020903 host galaxy, we derived the upper limit of the CO luminosity by assuming a velocity width of 180 km s^{-1} (Table 1). The assumption of this velocity width is identical to that of nondetection samples reported by Hatsukade et al. (2020a).

The upper limit of the molecular gas mass of the XRF 020903 host galaxy was derived from $M_{\text{gas}} =$

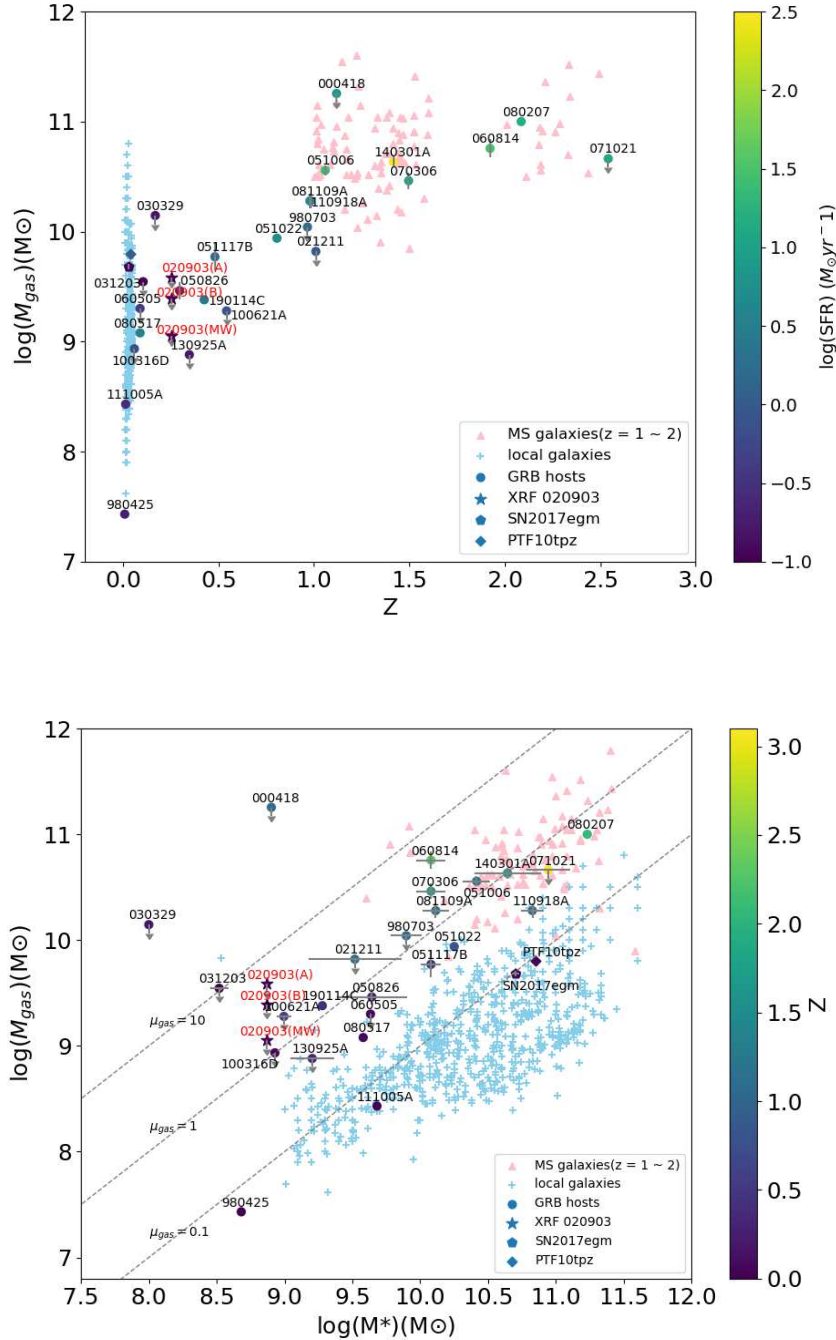


Figure 5. (Top) Redshift dependency of molecular gas mass (M_{gas}). Arrows represent 3σ upper limits. (Bottom) Comparison between molecular gas mass (M_{gas}) and stellar mass (M_*). Dashed lines show the molecular gas fractions ($\mu_{\text{gas}} = M_{\text{gas}}/M_*$) of 0.1, 1, and 10. Three upper limits of M_{gas} along to the metallicity-dependent CO-to- H_2 conversion factor are plotted for XRF 020903 (burst site as A, and remaining regions representative as B, and the value estimated with the galactic conversion factor as MW). For comparison, local galaxies (Bothwell et al. 2014; Saintonge et al. 2017; Tacconi et al. 2018) and $z \sim 1 - 2$ main-sequence galaxies are plotted. (Daddi et al. 2010; Magnelli et al. 2012; Tacconi et al. 2013; Seko et al. 2016).

$\alpha_{\text{CO}} L'_{\text{CO}(1-0)}$, where α_{CO} is the CO-to- H_2 conversion factor, including the contribution of the helium mass. We estimated the conversion factor by considering the dependency on the gas-phase metallicity and increasing α_{CO} as metallicity is decreased (e.g., Wilson 1995; Arimoto et al. 1996; Kennicutt & Evans 2012; Bolatto et al. 2013). The optical measurements indicate that all four regions of the XRF 020903 host galaxy are subsolar-metallicity ($12+\log(\text{O}/\text{H})=8.1-8.3$; Thorp & Levesque 2018). In the low-metallicity range, the conversion factor estimation becomes difficult, because the estimation methods have not yet been established. For example, the empirical relations between metallicity and α_{CO} of Genzel et al. (2012) and Bolatto et al. (2013) differed. Therefore, we adopted the harmonic mean of the recipes of Genzel et al. (2012) and Bolatto et al. (2013), similar to Hatsukade et al. (2020a). The converted upper limits of the gas mass were $M_{\text{gas}} < 3.9 \times 10^9 M_{\odot}$ with $\alpha_{\text{CO}} = 15 M_{\odot} (\text{K km s}^{-1} \text{ pc}^2)$ for region A and $M_{\text{gas}} < 2.5 \times 10^9 M_{\odot}$ with $\alpha_{\text{CO}} = 9.6 (\text{K km s}^{-1} \text{ pc}^2)$ for regions B, C, and D. The smaller upper limit of $M_{\text{gas}} < 1.1 \times 10^9$ was estimated by applying the galactic conversion factor of $\alpha_{\text{CO}}=4.4 (\text{K km s}^{-1} \text{ pc}^2)$; Bolatto et al. 2013). We compared the molecular gas mass of the XRF 020903 with other GRB and SLSN samples reported by Hatsukade et al. (2020a) as a function of redshift (Figure 5, top) and stellar mass (Figure 5, bottom). No violation was observed in the global trends of both the redshift and stellar mass. Additionally, we compared the local star-forming galaxies (Bothwell et al. 2014; Saintonge et al. 2017) and main-sequence galaxies at $z \sim 1 - 2$ (Daddi et al. 2010; Magdis et al. 2012; Magnelli et al. 2012; Tacconi et al. 2013; Seko et al. 2016). The upper limit of M_{gas} was consistent with those of local galaxies, in addition to the redshift. A comparable sample in the same stellar mass range did not exist. The limits for the hosts of XRF 020903 is lower than the gas mass fractions for the most gas-rich galaxies and some GRB hosts.

5.2. Molecular Gas Mass-SFR, Gas Fraction, and Depletion Timescale

The gas surface density was correlated to the SFR surface density, which is known as the Kennicutt-Schmidt relation (Schmidt 1959). The integration over the source region indicated a correlation between M_{gas} and the SFR. Figure 6 shows the relationship between the GRB host galaxies and the target. The SFR of XRF 020903 estimated using the H_{α} line as $2.65 M_{\odot} \text{ yr}^{-1}$ (Savaglio et al. 2009), was used. Three upper limits of M_{gas} for XRF 020903 (burst site as A, remaining regions representative as B, and the value estimated with the

galactic conversion factor as MW) were plotted, because the conversion factor of CO-to- H_2 depends on the metallicity, as described in §5.1. The GRB samples were those of Hatsukade et al. (2020a), who employed the SED fitting method to estimate the SFRs. The upper limit of the molecular gas mass of XRF 020903 indicates that the current event reflects the trend of GRB host galaxies. Additionally, we compared the local star-forming galaxies (Bothwell et al. 2014; Saintonge et al. 2017) and main-sequence galaxies at $z \sim 1 - 2$ (Tacconi et al. 2013; Seko et al. 2016). The upper limit of XRF 020903 was consistent with that of the local star-forming galaxies. When we adopted the galactic conversion factor of $\alpha_{\text{CO}}=4.4 (\text{K km s}^{-1} \text{ pc}^2)$, the limit indicated that the XRF 020903 host galaxy was at the smallest M_{gas} end in the same SFR range.

The majority of the GRB host galaxies were located on the molecular gas depletion timescale ($t_{\text{depl}}=M_{\text{gas}}/\text{SFR}$) of ~ 1 Gyr, whereas some hosts with lower redshift had a shorter gas depletion timescale (Figure 6). Hatsukade et al. (2020a) reported that GRB host galaxies tend to possess a higher molecular gas mass fraction (μ_{gas}) and a shorter gas depletion timescale (t_{depl}) than other star-forming galaxies at similar redshifts, particularly at $z < 1$. Figure 7 shows μ_{gas} and t_{depl} as a function of redshift. The lines in Figure 7 indicate the best-fit function of star-forming galaxies derived by Tacconi et al. (2018). For comparison, the distribution of the star-forming galaxies (Saintonge et al. 2017; Tacconi et al. 2018) is shown. Although the upper limit of μ_{gas} could not constrain the trend effectively, the limit of t_{depl} was consistent with the results of most of GRB samples (e.g., GRB 980703, GRB 021211, GRB 031203, GRB 050826, GRB 060814, GRB 070306, GRB 071021, GRB 081109A, GRB 110918A), and one of SLSN, PTF10tpz. As the upper limits were close to the best-fitted function of the star-forming galaxies, the depletion time, t_{depl} was consistent with or rather lower than the average of star-forming galaxies.

6. SUMMARY

Results of the ALMA dust continuum and CO observations of the XRF 020903 host galaxy were reported herein. The continuum observation provided the upper limit of the IR luminosity based on the template scaling method. The corresponding $\text{SFR} < 2.2 M_{\odot} \text{ yr}^{-1}$ was consistent with the measurement using the H_{α} emission line or rather small. Based on the CO observation, $M_{\text{gas}} < 3.9 \times 10^9 M_{\odot}$ for the burst site by applying the metallicity-dependent CO-to- H_2 conversion factor. The gas mass matched with the global trend of the GRB host galaxies, in addition to the redshift and stellar mass. As

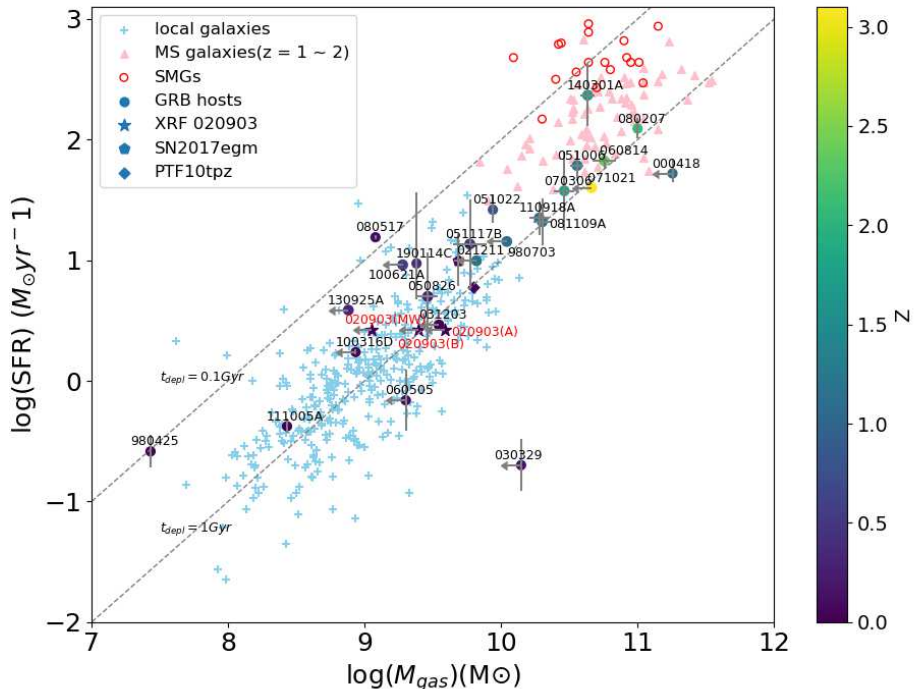


Figure 6. Molecular gas mass (M_{gas}) compared with SFR. Dashed lines indicate the gas depletion timescale of 0.1 and 1 Gyr (see Table 1). Three upper limits of M_{gas} and metallicity-dependent CO-to- H_2 conversion factor are plotted for XRF 020903 (burst site as A, remaining regions representative as B, and the value estimated with the galactic conversion factor as MW). For comparison, local galaxies (Bothwell et al. 2014; Saintonge et al. 2017), $z \sim 1 - 2$ main-sequence galaxies (Tacconi et al. 2013; Seko et al. 2016), and SMGs Bothwell et al. (2013) are plotted.

one of the potential common properties of GRB host galaxies, we confirmed that the gas depletion timescale is equivalent to those of the GRBs and SLSNs at the same redshift range (i.e., GRB 031203, GRB 050826, and PTF10tpz). These results indicate the similar properties of the XRF 020903 host galaxy to those of GRB host galaxies and supports the identical origins of XRF 020903 and GRBs.

ACKNOWLEDGMENTS

This paper makes use of the following ALMA data: ADS/JAO.ALMA#2015.1.01254 and #2016.1.01333.S. ALMA is a partnership of ESO (representing its member states), NSF (USA), and NINS (Japan), together with NRC (Canada), MOST and ASIAA (Taiwan), and KASI (Republic of Korea), in cooperation with the Republic of Chile. The Joint ALMA Observatory is operated by ESO, AUI/NRAO, and NAOJ. This research has made use of the GHostS database (www.grbhosts.org), which is partly funded by Spitzer/NASA grant RSA agreement No. 1287913. Based on observations made with the NASA/ESA Hubble Space Telescope and obtained from the Hubble Legacy Archive, which is a collaboration between the Space Telescope Science Institute (STScI/NASA), the Space Telescope European Coordinating Facility (ST-ECF/ESA), and the Canadian Astronomy Data Centre (CADC/NRC/CSA). This work is supported by the Ministry of Science and Technology of Taiwan grants MOST 105-2112-M-008-013-MY3 (Y.U.).

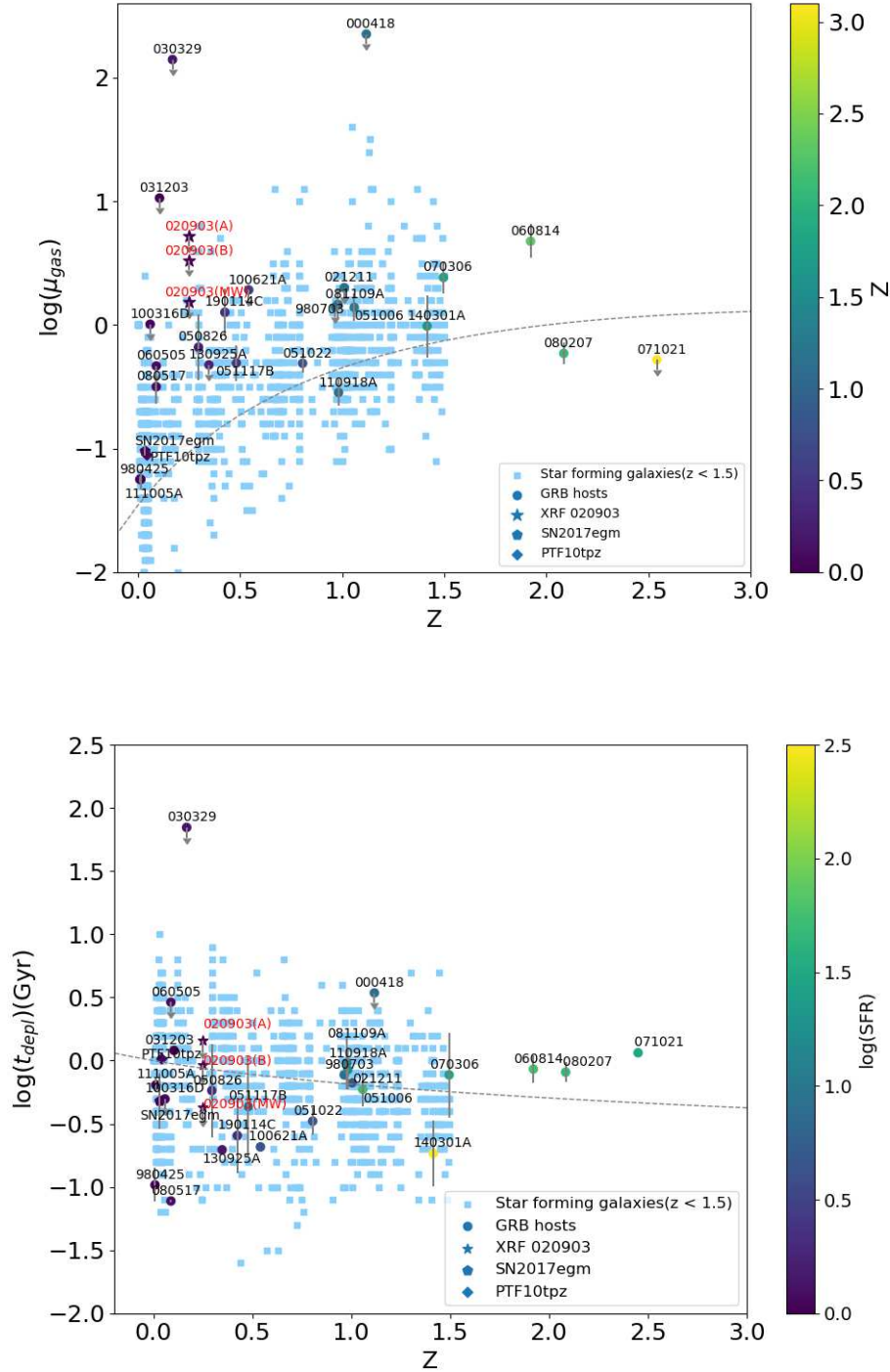


Figure 7. Molecular gas fraction (μ_{gas} ; top) and molecular gas depletion timescale (t_{depl} ; bottom) compared with the redshift. Three upper limits and metallicity-dependent CO-to-H₂ conversion factor are plotted for XRF 020903 (burst site as A, remaining regions representative as B, and the value estimated with the galactic conversion factor as MW). The dashed line represents the best-fit line for the main-sequence galaxies derived by Tacconi et al. (2018). Distribution of star-forming galaxies (Tacconi et al. 2018) is plotted for comparison.

Table 1. XRF 020903 and GRBs host galaxies samples

Event	Redshift	Frequency (GHz)	Flux (mJy)	L_{IR} (L_{\odot})	SFR ($M_{\odot} \text{ yr}^{-1}$)	CO Luminosity ($\text{K km s}^{-1} pc^2$)	Gas Mass (M_{\odot})	Reference
GRB 980425	0.0085	106.8	0.77 ± 0.26	3.53×10^9	0.60	2.3×10^6	2.7×10^7	Michałowski et al. (2018)
GRB 980703	0.966	234.5	< 0.081	$< 1.75 \times 10^{11}$	< 29.7	$< 4.0 \times 10^8$	$< 1.1 \times 10^{10}$	Hatsukade et al. (2020a)
GRB 000418	1.1183	—	—	—	—	$< 1.0 \times 10^{10}$	$< 1.8 \times 10^{11}$	Hatsukade et al. (2011)
GRB 020819B	1.9621	245.1	0.14 ± 0.03	6.23×10^{11}	105.9	—	—	Hatsukade et al. (2014)
XRF 020903	0.251	97.2	< 0.032	$< 1.28 \times 10^{11}$	< 21.7	$< 2.6 \times 10^8$	$< 1.1 \times 10^9$	This work
		233.0	< 0.061	$< 1.30 \times 10^{10}$	< 2.21	—	—	This work
GRB 021004	2.330	345.0	< 0.354	$< 3.13 \times 10^{11}$	< 53.1	—	—	Wang et al. (2012)
GRB 021211	1.010	229.8	< 0.063	$< 1.5 \times 10^{11}$	< 25.8	$< 2.9 \times 10^8$	$< 6.6 \times 10^9$	Hatsukade et al. (2020a)
GRB 030329	0.1685	—	—	—	—	$< 6.9 \times 10^8$	$< 1.4 \times 10^{10}$	Endo et al. (2007)
GRB 031203	0.105	312.8	< 2.410	$< 4.5 \times 10^9$	< 0.8	$< 1.8 \times 10^8$	$< 3.5 \times 10^9$	Hatsukade et al. (2020a)
GRB 050401	2.900	343.5	< 0.67	$< 7.30 \times 10^{11}$	< 124.2	—	—	This work
GRB 050709	0.1606	233.0	< 0.05	$< 5.97 \times 10^9$	< 1.0	—	—	This work
GRB 050826	0.296	266.8	< 0.084	$< 2.4 \times 10^{10}$	< 4.1	$(2.8 \pm 0.5) \times 10^8$	$(2.9 \pm 0.5) \times 10^9$	Hatsukade et al. (2020a)
GRB 050915A	2.527	343.5	0.37 ± 0.13	4.09×10^{11}	69.5	—	—	This work
GRB 051006	1.059	223.9	0.078 ± 0.024	2.0×10^{11}	33.8	$(2.7 \pm 0.3) \times 10^9$	$(3.6 \pm 0.4) \times 10^{10}$	Hatsukade et al. (2020a)
GRB 051022	0.806	256.1	< 1.6	$< 6.25 \times 10^{12}$	< 1062	4.2×10^8	8.7×10^9	Hatsukade et al. (2014)
GRB 051117B	0.481	225.3	0.069 ± 0.020	8.0×10^{10}	13.7	$(9.1 \pm 0.3) \times 10^8$	$(5.9 \pm 1.7) \times 10^9$	Hatsukade et al. (2020a)
GRB 060505	0.089	—	—	—	—	$< 4.2 \times 10^8$	$< 2.0 \times 10^9$	Michałowski et al. (2018)
GRB 060814	1.923	343.5	< 0.063	$< 6.8 \times 10^{11}$	< 115.1	$(2.7 \pm 0.5) \times 10^9$	$(5.7 \pm 1.1) \times 10^{10}$	Hatsukade et al. (2020a)
GRB 070306	1.496	343.5	< 0.036	$< 5.7 \times 10^{11}$	< 96.8	$(2.2 \pm 0.4) \times 10^9$	$(2.9 \pm 0.5) \times 10^{10}$	Hatsukade et al. (2020a)
GRB 070521	2.087	680.0	< 3.12	$< 7.30 \times 10^{11}$	< 124.2	—	—	Hashimoto et al. (2019)
GRB 070802	2.450	343.5	0.30 ± 0.11	2.88×10^{11}	49.0	—	—	This work
GRB 071021	2.542	133.6	< 0.042	$< 6.8 \times 10^{11}$	< 115.1	$< 1.3 \times 10^9$	$< 4.6 \times 10^{10}$	Hatsukade et al. (2020a)
GRB 080207	2.086	142.5	0.11 ± 0.03	2.46×10^{12}	417.5	1.7×10^{10}	1.0×10^{11}	Hatsukade et al. (2019)
GRB 080517	0.0889	—	—	—	—	1.5×10^8	1.2×10^9	Stanway et al. (2015)
GRB 081109A	0.979	233.0	< 0.087	$< 2.0 \times 10^{11}$	< 33.8	$(1.4 \pm 0.2) \times 10^9$	$(2.0 \pm 0.3) \times 10^{10}$	Hatsukade et al. (2020a)
GRB 081221	2.260	343.5	0.88 ± 0.09	1.13×10^{12}	192.5	—	—	This work
GRB 090423	8.230	222.0	< 0.036	$< 4.50 \times 10^{10}$	< 7.6	—	—	Berger et al. (2014)
GRB 100316D	0.059	—	—	—	—	$< 1.4 \times 10^8$	$< 8.6 \times 10^8$	Michałowski et al. (2018)
GRB 100621A	0.542	224.3	< 0.066	$< 5.7 \times 10^{10}$	< 9.8	$< 1.4 \times 10^8$	$< 1.9 \times 10^9$	Hatsukade et al. (2020a)
GRB 110918A	0.982	232.3	0.097 ± 0.020	2.4×10^{11}	41.4	$(1.7 \pm 0.2) \times 10^9$	$(1.9 \pm 0.3) \times 10^{10}$	Hatsukade et al. (2020a)
GRB 111005A	0.013	—	—	—	—	4.4×10^7	2.7×10^8	Michałowski et al. (2018)
GRB 111123A	3.152	343.5	0.96 ± 0.10	1.13×10^{12}	192.5	—	—	This work
GRB 120624B	2.197	343.5	0.35 ± 0.12	3.68×10^{11}	62.5	—	—	This work
GRB 130606A	5.913	265.0	< 0.354	$< 5.69 \times 10^{11}$	< 96.8	—	—	This work
GRB 130925A	0.347	256.5	< 0.096	$< 3.8 \times 10^{10}$	< 6.5	$< 7.6 \times 10^7$	$< 7.6 \times 10^8$	Hatsukade et al. (2020a)
GRB 131030	1.293	345.0	< 0.12	$< 6.5 \times 10^{11}$	< 11.1	—	—	Huang et al. (2017)

Table 1 *continued*

Table 1 (*continued*)

Event	Redshift	Frequency (GHz)	Flux (mJy)	L_{IR} (L_{\odot})	SFR ($M_{\odot} \text{ yr}^{-1}$)	CO Luminosity ($\text{K km s}^{-1} pc^2$)	Gas Mass (M_{\odot})	Reference
GRB 140301A	1.416	143.2	<0.039	$< 5.7 \times 10^{11}$	<96.8	$(5.5 \pm 0.6) \times 10^9$	$(4.3 \pm 0.5) \times 10^{10}$	Hatsukade et al. (2020a)
GRB 190114C	0.425	—	—	—	—	1.54×10^8	2.4×10^9	de Ugarte Postigo et al. (2020)
SN2017egm	0.031	—	—	—	—	$(1.1 \pm 0.1) \times 10^9$	$(4.8 \pm 0.3) \times 10^9$	Hatsukade et al. (2020b)
PTF10tpz	0.040	—	—	—	—	$(1.45 \pm 0.03) \times 10^9$	6.3×10^9	Arabsalmani et al. (2019)

Facilities: ALMA, HST

Software: CASA (v4.7.0-1; McMullin et al. 2007)

REFERENCES

- Alexander, K. D., Berger, E., Fong, W., et al. 2017, *ApJL*, 848, L21
- Amati, L., O’Brien, P., Götz, D., et al. 2018, *Advances in Space Research*, 62, 191. doi:10.1016/j.asr.2018.03.010
- Arabsalmani, M., Roychowdhury, S., Renaud, F., et al. 2019, *ApJ*, 882, 31. doi:10.3847/1538-4357/ab2897
- Arabsalmani, M., Renaud, F., Roychowdhury, S., et al. 2020, *ApJ*, 899, 165. doi:10.3847/1538-4357/aba3c0
- Arimoto, N., Sofue, Y., & Tsujimoto, T. 1996, *PASJ*, 48, 275. doi:10.1093/pasj/48.2.275
- Bellm, E. C., Barrière, N. M., Bhalerao, V., et al. 2014, *ApJL*, 784, L19. doi:10.1088/2041-8205/784/2/L19
- Berger, E., Zauderer, B. A., Chary, R.-R., et al. 2014, *ApJ*, 796, 96. doi:10.1088/0004-637X/796/2/96
- Bersier, D., Fruchter, A. S., Strolger, L.-G., et al. 2006, *ApJ*, 643, 284. doi:10.1086/502640
- Bolatto, A. D., Warren, S. R., Leroy, A. K., et al. 2013, *Nature*, 499, 450. doi:10.1038/nature12351
- Bolatto, A. D., Wolfire, M., & Leroy, A. K. 2013, *ARA&A*, 51, 207. doi:10.1146/annurev-astro-082812-140944
- Bothwell, M. S., Smail, I., Chapman, S. C., et al. 2013, *MNRAS*, 429, 3047. doi:10.1093/mnras/sts562
- Bothwell, M. S., Wagg, J., Ciccone, C., et al. 2014, *MNRAS*, 445, 2599. doi:10.1093/mnras/stu1936
- Buat, V. & Xu, C. 1996, *A&A*, 306, 61
- Chary, R., & Elbaz, D. 2001, *ApJ*, 556, 562
- Chen, W. J., Urata, Y., Huang, K., et al. 2020, *ApJL*, 891, L15. doi:10.3847/2041-8213/ab76d4
- Coppejans, D. L., Margutti, R., Guidorzi, C., et al. 2018, *ApJ*, 856, 56. doi:10.3847/1538-4357/aab36e
- Covino, S., Malesani, D., Israel, G. L., et al. 2006, *A&A*, 447, L5. doi:10.1051/0004-6361/200500228
- Daddi, E., Bournaud, F., Walter, F., et al. 2010, *ApJ*, 713, 686. doi:10.1088/0004-637X/713/1/686
- de Ugarte Postigo, A., Thöne, C. C., Martín, S., et al. 2020, *A&A*, 633, A68. doi:10.1051/0004-6361/201936668
- Endo, A., Kohno, K., Hatsukade, B., et al. 2007, *ApJ*, 659, 1431. doi:10.1086/512764
- Evans, P. A., Willingale, R., Osborne, J. P., et al. 2014, *MNRAS*, 444, 250. doi:10.1093/mnras/stu1459
- Fox, D. B., Frail, D. A., Price, P. A., et al. 2005, *Nature*, 437, 845. doi:10.1038/nature04189
- Gal-Yam, A., Ofek, E. O., Poznanski, D., et al. 2006, *ApJ*, 639,
- Godet, O., Paul, J., Wei, J. Y., et al. 2012, *Proc. SPIE*, 8443, 84431O. doi:10.1117/12.925171
- Greiner, J., Hartmann, D. H., Voges, W., et al. 2000, *A&A*, 353, 998
- Greiner, J., Yu, H.-F., Krühler, T., et al. 2014, *A&A*, 568, A75. doi:10.1051/0004-6361/201424250
- Grindlay, J. E. 1999, *ApJ*, 510, 710
- Haggard, D., Nynka, M., Ruan, J. J., et al. 2017, *ApJL*, 848, L25
- Hammer, F., Flores, H., Schaerer, D., et al. 2006, *A&A*, 454, 103. doi:10.1051/0004-6361:20064823
- Han, X. H., Hammer, F., Liang, Y. C., et al. 2010, *A&A*, 514, A24. doi:10.1051/0004-6361/200912475
- Hashimoto, T., Hatsukade, B., Goto, T., et al. 2019, *MNRAS*, 488, 5029. doi:10.1093/mnras/stz2034
- Hatsukade, B., Kohno, K., Endo, A., et al. 2011, *ApJ*, 738, 33. doi:10.1088/0004-637X/738/1/33
- Hatsukade, B., Ohta, K., Endo, A., et al. 2014, *Nature*, 510, 247. doi:10.1038/nature13325
- Hatsukade, B., Hashimoto, T., Kohno, K., et al. 2019, *ApJ*, 876, 91. doi:10.3847/1538-4357/ab1649
- Hatsukade, B., Ohta, K., Hashimoto, T., et al. 2020, *ApJ*, 892, 42. doi:10.3847/1538-4357/ab7992
- Hatsukade, B., Morokuma-Matsui, K., Hayashi, M., et al. 2020, *PASJ*, 72, L6. doi:10.1093/pasj/psaa052
- Heise, J., Zand, J. I., Kippen, R. M., et al. 2001, *Gamma-ray Bursts in the Afterglow Era*, 16. doi:10.1007/10853853_4
- Heise, J. 2003, *Gamma-Ray Burst and Afterglow Astronomy 2001: A Workshop Celebrating the First Year of the HETE Mission*, 662, 229
- Hjorth, J., Watson, D., Fynbo, J. P. U., et al. 2005, *Nature*, 437, 859. doi:10.1038/nature04174
- Huang, Y. F., Dai, Z. G., & Lu, T. 2002, *MNRAS*, 332, 735
- Huang, K., Urata, Y., Takahashi, S., et al. 2017, *PASJ*, 69, 20
- Huang, K., Shimoda, J., Urata, Y., et al. 2019, *ApJL*, 878, L25. doi:10.3847/2041-8213/ab23fd
- Huang, Y.-J., Urata, Y., Huang, K., et al. 2020, *ApJ*, 897, 69. doi:10.3847/1538-4357/ab8f9a
- Ioka, K., & Nakamura, T. 2018, *Progress of Theoretical and Experimental Physics*, 2018, 043E02
- Izzo, L., de Ugarte Postigo, A., Maeda, K., et al. 2019, *Nature*, 565, 324. doi:10.1038/s41586-018-0826-3
- Izzo, L., Auchettl, K., Hjorth, J., et al. 2020, *A&A*, 639, L11. doi:10.1051/0004-6361/202038152

- Jin, Z.-P., Li, X., Wang, H., et al. 2018, *ApJ*, 857, 128
- Kathirgamaraju, A., Barniol Duran, R., & Giannios, D. 2018, *MNRAS*, 473, L121
- Kennicutt, R. C. & Evans, N. J. 2012, *ARA&A*, 50, 531. doi:10.1146/annurev-astro-081811-125610
- Kennicutt, R. C., Jr. 1998, *ARA&A*, 36, 189
- Kippen, R. M., Woods, P. M., Heise, J., et al. 2002, *APS April Meeting Abstracts*
- Lamb, G. P., & Kobayashi, S. 2018, *MNRAS*, 478, 733
- Lamb, D. Q., Donaghy, T. Q., & Graziani, C. 2005, *ApJ*, 620, 355. doi:10.1086/426099
- Lamb, G. P., Lyman, J. D., Levan, A. J., et al. 2019, *ApJL*, 870, L15
- Law, C. J., Gaensler, B. M., Metzger, B. D., et al. 2018, *ApJL*, 866, L22
- Lazzati, D., López-Cámara, D., Cantiello, M., et al. 2017, *ApJL*, 848, L6
- Levesque, E. M., Berger, E., Kewley, L. J., et al. 2010, *AJ*, 139, 694. doi:10.1088/0004-6256/139/2/694
- Levinson, A., Ofek, E. O., Waxman, E., et al. 2002, *ApJ*, 576, 923
- Lyman, J. D., Lamb, G. P., Levan, A. J., et al. 2018, *NatAs*, 2, 751
- Magdis, G. E., Daddi, E., Béthermin, M., et al. 2012, *ApJ*, 760, 6. doi:10.1088/0004-637X/760/1/6
- Magnelli, B., Saintonge, A., Lutz, D., et al. 2012, *A&A*, 548, A22. doi:10.1051/0004-6361/201220074
- Marcote, B., Nimmo, K., Salafia, O. S., et al. 2019, *ApJL*, 876, L14
- McMullin, J. P., Waters, B., Schiebel, D., Young, W., & Golap, K. 2007, *adass*, 376, 127
- Michałowski, M. J., Karska, A., Rizzo, J. R., et al. 2018, *A&A*, 617, A143. doi:10.1051/0004-6361/201833250
- Murguia-Berthier, A., Ramirez-Ruiz, E., Kilpatrick, C. D., et al. 2017, *ApJL*, 848, L34
- Nicholl, M., Berger, E., Margutti, R., et al. 2017, *ApJL*, 845, L8. doi:10.3847/2041-8213/aa82b1
- Pastorello, A., Smartt, S. J., Botticella, M. T., et al. 2010, *ApJL*, 724, L16. doi:10.1088/2041-8205/724/1/L16
- Perley, D. A., Krühler, T., Schady, P., et al. 2017, *MNRAS*, 465, L89. doi:10.1093/mnras/17221
- Piro, L., Troja, E., Gendre, B., et al. 2014, *ApJL*, 790, L15. doi:10.1088/2041-8205/790/2/L15
- Racusin, J. L., Liang, E. W., Burrows, D. N., et al. 2009, *ApJ*, 698, 43
- Rau, A., Greiner, J., & Schwarz, R. 2006, *A&A*, 449, 79
- Saintonge, A., Catinella, B., Tacconi, L. J., et al. 2017, *ApJS*, 233, 22. doi:10.3847/1538-4365/aa97e0
- Sakamoto, T., Lamb, D. Q., Graziani, C., et al. 2004, *ApJ*, 602, 875
- Sakamoto, T., Lamb, D. Q., Kawai, N., et al. 2005, *ApJ*, 629, 311. doi:10.1086/431235
- Savaglio, S., Glazebrook, K., & Le Borgne, D. 2009, *ApJ*, 691, 182. doi:10.1088/0004-637X/691/1/182
- Schmidt, M. 1959, *ApJ*, 129, 243. doi:10.1086/146614
- Seko, A., Ohta, K., Yabe, K., et al. 2016, *ApJ*, 819, 82. doi:10.3847/0004-637X/819/1/82
- Shirasaki, Y., Kawai, N., Yoshida, A., et al. 2003, *PASJ*, 55, 1033. doi:10.1093/pasj/55.5.1033
- Soderberg, A. M., Kulkarni, S. R., Berger, E., et al. 2004, *ApJ*, 606, 994
- Soderberg, A. M., Kulkarni, S. R., Fox, D. B., et al. 2005, *ApJ*, 627, 877. doi:10.1086/430405
- Solomon, P. M. & Vanden Bout, P. A. 2005, *ARA&A*, 43, 677. doi:10.1146/annurev.astro.43.051804.102221
- Stanway, E. R., Levan, A. J., Tanvir, N. R., et al. 2015, *ApJL*, 798, L7. doi:10.1088/2041-8205/798/1/L7
- Tacconi, L. J., Neri, R., Genzel, R., et al. 2013, *ApJ*, 768, 74. doi:10.1088/0004-637X/768/1/74
- Tacconi, L. J., Genzel, R., Saintonge, A., et al. 2018, *ApJ*, 853, 179. doi:10.3847/1538-4357/aaa4b4
- Tanvir, N. R., Fox, D. B., Levan, A. J., et al. 2009, *Nature*, 461, 1254. doi:10.1038/nature08459
- Thorp, M. D. & Levesque, E. M. 2018, *ApJ*, 856, 36. doi:10.3847/1538-4357/aab093
- Totani, T., Aoki, K., Hattori, T., et al. 2014, *PASJ*, 66, 63. doi:10.1093/pasj/psu032
- Totani, T., Aoki, K., Hattori, T., et al. 2016, *PASJ*, 68, 15. doi:10.1093/pasj/psv123
- Troja, E., Piro, L., Ryan, G., et al. 2018, *MNRAS*, 478, L18
- Troja, E., van Eerten, H., Ryan, G., et al. 2019, *MNRAS*, 489, 1919
- Urata, Y., Huang, K., Yamazaki, R., & Sakamoto, T. 2015, *ApJ*, 806, 222
- Urata, Y., Toma, K., Huang, K., et al. 2019, *ApJL*, 884, L58
- Villasenor, J. S., Lamb, D. Q., Ricker, G. R., et al. 2005, *Nature*, 437, 855. doi:10.1038/nature04213
- Wang, W.-H., Chen, H.-W., & Huang, K.-Y. 2012, *ApJL*, 761, L32. doi:10.1088/2041-8205/761/2/L32
- Wheeler, J. C., Chatzopoulos, E., Vinkó, J., et al. 2017, *ApJL*, 851, L14. doi:10.3847/2041-8213/aa9d84
- Wilson, C. D. 1995, *ApJL*, 448, L97. doi:10.1086/309615
- Yamazaki, R., Ioka, K., & Nakamura, T. 2002, *ApJL*, 571, L31
- Yasuda, T., Urata, Y., Enomoto, J., et al. 2017, *MNRAS*, 466, 4558. doi:10.1093/mnras/stw3130
- Yonetoku, D., Mihara, T., Doi, A., et al. 2020, *Proc. SPIE*, 11444, 114442Z. doi:10.1117/12.2560603
- Zhang, B., Dai, X., Lloyd-Ronning, N. M., & Mészáros, P. 2004, *ApJL*, 601, L119